JOURNAL OF CATALYSIS 115, 310–318 (1989)

The Decomposition of Unsaturated Hydrocarbons on Small Pd Particles

W. G. DURRER,* H. POPPA,† AND J. T. DICKINSON*

*Department of Physics, Washington State University, Pullman, Washington 99164-2814, and †Stanford–NASA Joint Institute for Surface and Microstructure Research, NASA–Ames Research Center, Moffett Field, California 94035

Received January 4, 1988; revised July 26, 1988

The decomposition of propylene, acetylene, and methylacetylene on the surfaces of small supported Pd particles has been investigated using flash thermal desorption of CO, Auger electron spectroscopy, and transmission electron microscopy. Pd crystallite size distributions averaged 2 to 14 nm in diameter. Samples were prepared by vapor deposition of high-purity Pd onto clean mica surfaces cleaved and annealed under ultrahigh vacuum. Our results reveal that (a) the hydrocarbons decompose at certain sites, contaminating such sites to prevent subsequent reaction or CO adsorption and (b) the surface density of decomposition sites is particle size dependent, being greater on smaller particles. A simple kinetic model and computerized curve fitting are used to compare the behavior of the above gases with that of ethylene presented in previous work. This analysis shows a significant difference in decomposition properties between those hydrocarbons containing a double C–C bond and those with a triple C–C bond.

INTRODUCTION

This paper presents a study of the deactivation of CO adsorption sites caused by hydrocarbon decomposition on systems of small supported Pd particles and the dependence of this deactivation on the structure of the hydrocarbon molecules, distribution and nature of surface reaction sites, and average particle diameter. We employed transmission electron microscopy to determine particle size distributions, Auger electron spectroscopy to monitor the buildup of carbonaceous species, and flash thermal desorptions of CO to probe changes in the "active" surface area of highly dispersed Pd films exposed to successive small doses of hydrocarbon gases. The selection of gases used in the experiments allowed us to determine the extent to which hydrocarbon–particle interactions change with two important variations in hydrocarbon molecular structure. First, presented below, the comparison between alkenes and alkynes allows us to draw conclusions from our data about differences in surface distributions of decomposition sites for the two different (double vs triple) carbon–carbon bond structures. Second, similarities between the cases of ethene and propene and between ethyne and propyne will be shown to provide important information about the nature of the contamination of CO adsorption sites.

EXPERIMENTAL

The experiments were performed in a dual-chamber UHV system (*1*) at a base pressure of 1×10^{-10} Torr. The Pd particle deposits to be studied were created by electron beam evaporation of the metal (99.99% purity) at a rate of 1.2 nm/min onto a clean mica surface held at a temperature of 600 K in a cylindrical oven cut with a small rectangular hole to admit the evaporated Pd flux. The amount of metal deposited was controlled by timing a manually operated shutter and was monitored by means of a quartz crystal microbalance. For the sake of comparison with an earlier ethylene study (*2*), the same four metal deposition thicknesses were prepared, namely, 0.06, 0.31, 0.61, and 1.2 nm of average Pd film thickness. Average particle sizes were de-

0021-9517/89 $3.00

termined directly by transmission electron microscopy using techniques described elsewhere (*1–3*). Tests of particles that had been through several cycles of heating to 480 K showed no evidence of sintering.

Each new film substrate was obtained by cleaving a mica block under ultrahigh vacuum. The mica surface was then annealed in the deposition oven at 800 K for 15 min and the temperature decreased to 600 K for the deposit.

The design of the UHV system provided for linear translation of the freshly prepared sample from the deposition oven and chamber to a chamber equipped for Auger electron spectroscopy and flash thermal desorption. After an initial Auger analysis, the sample was given a saturation dose of 6 $\times$ 10^{-6} Torr-sec (6 Langmuirs) of CO at a pressure of 1 $\times$ 10^{-7} Torr. Repeated tests with the QMS during adsorption showed no evidence that the CO dose displaced any hydrocarbon from the surface. The sample at the time of adsorption was slightly above room temperature, 320 K, according to previously measured heating and cooling curves (*1*). Flash thermal desorption of CO was achieved by rapidly inserting the sample into a desorption oven held at a constant temperature of 620 K; the sample was removed as soon as its temperature reached 480 K. A small hole in this desorption oven allowed a direct line of sight between the sample and the mass spectrometer. A CO flash adsorption/desorption was initially performed on the clean Pd particles to normalize the original CO adsorption "area." (Details of the behavior of CO on the Pd particles supported on mica can be found in Ref. (*1*).) Elsewhere (*4*) we have shown that for the conditions used in this study, no evidence of CO decomposition on the Pd particles was observed. This behavior is now known to be controlled by the particle morphology which under the current growth conditions was not inducive to CO disproportionation. Thus, repeated CO adsorption/desorption cycles yielded no loss in CO adsorption "area."

One cycle of the experiment consisted of (a) Auger analysis immediately after the previous CO desorption (the average temperature during the AES measurements was 370 K); (b) cooling for 15 min to adsorption temperature; (c) a small, reproducible dose of the hydrocarbon under study; and (d) a saturation dose of CO followed by (e) the next flash thermal desorption.

For the AES measurements, we employed a Varian single-pass cylindrical mirror analyzer with an integral, axial 3-kV electron gun. A beam current of 5 μA and a primary energy of 1500 eV were used. Peaks were recorded in the $dN(E)/dE$ mode. Each AES analysis included a high-sensitivity sweep of the energy range from approximately 225 eV to 360 eV in order to measure both Pd peaks and the overlapping carbon peak. The practice of obtaining Auger spectra immediately after CO desorption minimized the effects of contamination from electron beam-induced decomposition of background gases.

RESULTS

Flash Thermal Desorption

A CO desorption series resulting from the above sequence of procedures is illustrated in Fig. 1. The case shown is for the largest Pd particle size studied (average diameter about 14 nm) with successive 0.091 Langmuir exposures to propylene. The areas under these curves, normalized with respect to the area of the first desorption, were plotted as a function of cumulative propylene exposure in Fig. 2. Similar to results using ethylene treatment cycles (*2*), we observed the following:

(a) A loss of CO adsorption area with repeated hydrocarbons exposure cycles.

(b) An initial slope which will be shown to be proportional to the average surface concentration of hydrocarbon decomposition sites on the particles.

(c) A curve decreasing area loss per hydrocarbon exposure cycle.

(d) An asymptotic value (dashed line)

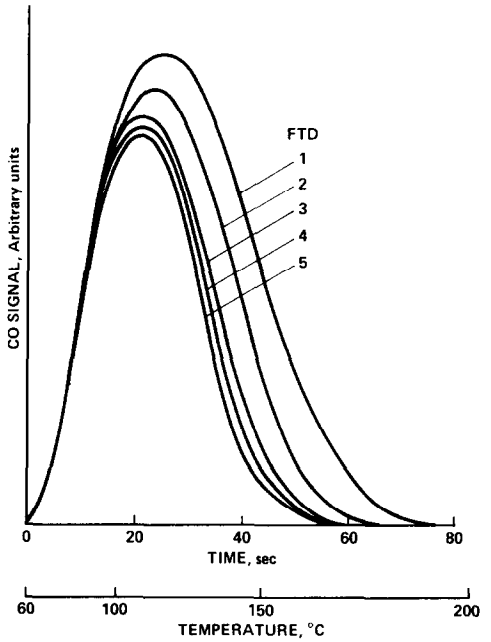

FIG. 1. CO desorption curves for a sample with average Pd particle diameter of 14 nm. The first curve was obtained after exposing the clean particles to a saturation dose (6×10^{-6} Torr-sec) of CO at 320 K. Each subsequent curve is a result of exposure of the same sample to 0.091 Langmuir of propylene at 320 K followed by CO saturation and desorption.

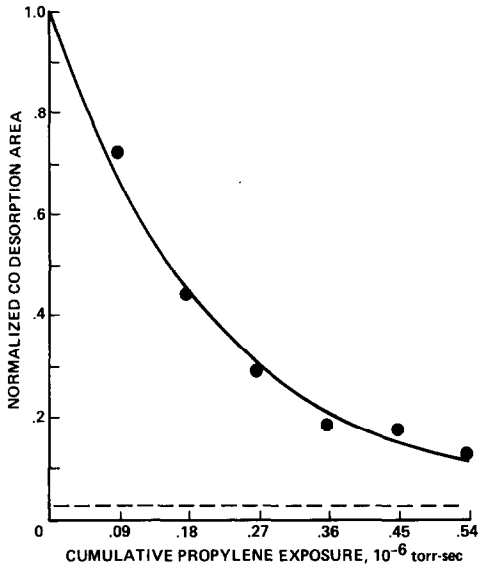

FIG. 2. Normalized areas from the CO desorption series of Fig. 1 plotted vs cumulative propylene exposure. The solid curve is a least-squares fit of $y = (1 - B) \exp(-kx) + B$ to the data, for which $k = 4.6$ $(10^{-6}$ Torr-sec$)^{-1}$, $B = 0.36$. The dashed line shows the asymptotic value of B.

representing that fraction of the total CO adsorbing area that remains unblocked by the treatment.

Both propylene and ethylene data could be fit by a function of the form

$$y = (1 - B) \exp(-kx) + B. \qquad (1)$$

(In our case, y represents the normalized CO adsorption area and x represents the cumulative hydrocarbon dose.) By use of a nonlinear least-squares computer program, a best fit was obtained for the propylene data (solid line in Fig. 2) with the values $k = 4.6$, $B = 0.36$. The physical significance of these values will be discussed in greater detail later.

Figure 3 shows the accumulated data for the four different particle sizes. Clearly, over this range of size, there is a particle size dependence observed. Similar data for

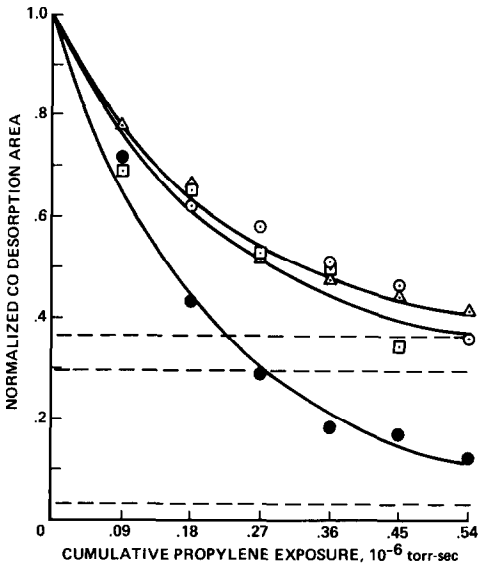

FIG. 3. Normalized CO desorption area vs cumulative propylene exposure for four different particle sizes: 2.0 nm (solid circles), 5.6 nm (squares), 9.0 nm (open circles), and 14 nm (triangles) average diameter. Again, the solid curves are least-squares fits of $y = (1 - B) \exp(-kx) + B$ and the dashed lines are the asymptotes.

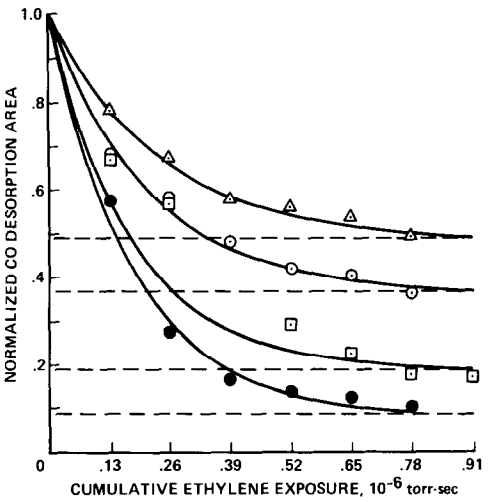

FIG. 4. Normalized CO desorption area vs cumulative ethylene exposure for average particle diameters 2.0 nm (solid circles), 5.6 nm (squares), 9.0 nm (open circles), and 14 nm (triangles), with least-squares fits of $y = (1 - B)\exp(-kx) + B$ (solid curves) and asymptotes (dashed lines).

the same average particle sizes for ethylene were seen in Fig. 4, showing very similar variations with particle size. In Figs. 3 and 4, the solid lines are the computer fits to Eq. (1).

Similar experiments using molecules containing a triple carbon–carbon bond were performed. Results for acetylene and methylacetylene are shown in Figs. 5 and 6, respectively. Again, there are significant losses in the CO adsorbing areas with repeated hydrocarbon doses. In contrast to the alkenes, the asymptotic values for all particle sizes are essentially zero. In spite of some deviations for different size categories, we see that this very simple model does fairly well at fitting the data. The deviations may in fact be due to the range of particle size within each metal exposure.

In Eq. (1), k is a measure of the overall ability of the deposited particles to transform the hydrocarbon to a surface species which blocks CO adsorption. The exponential decay suggests that the probability of this transformation appears to be directly proportional to the number of some form of open sites. From our least-squares analyses, we obtain values of k for a given hydrocarbon and particle size. In Fig. 7, we plot k

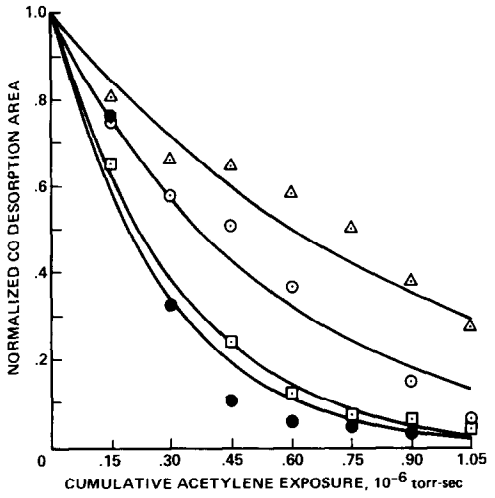

FIG. 5. Normalized CO desorption area vs cumulative acetylene exposure for average particle diameters 2.0 nm (solid circles), 5.6 nm (squares), 9.0 nm (circles), and 14 nm (triangles). Here, the best-fit exponentials (solid curves) have asymptotes at zero: $y = \exp(-kx)$.

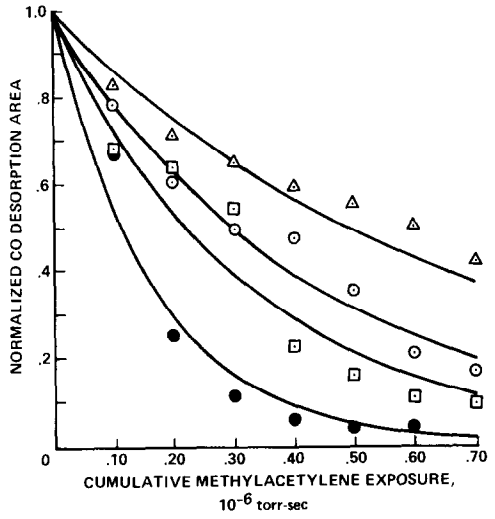

FIG. 6. Normalized CO desorption area vs cumulative methylacetylene exposure for average particle diameters 2.0 nm (solid circles), 5.6 nm (squares), 9.0 nm (circles), and 14 nm (triangles), with least-squares fits to $y = \exp(-kx)$ (solid curves).

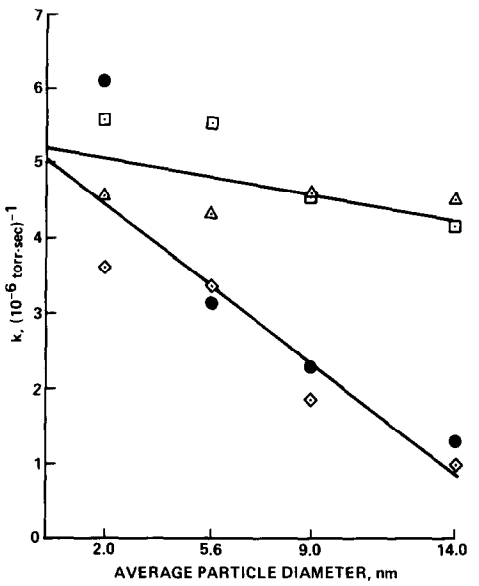

FIG. 7. Decay constant, k, vs particle size for ethylene (squares), propylene (triangles), acetylene (diamonds), and methylacetylene (solid circles) from least-squares fits of Figs. 3–6. Note the strong decrease in k with increasing particle size for the alkynes.

vs average particle size for the four hydrocarbons studied. Note that the two alkenes have very similar behavior. Their average dependence is represented by the slightly downward sloping straight line. The two alkynes also show nearly identical behavior. In contrast to the alkenes, k varies with particle size in a much stronger fashion for the alkynes.

The absolute values of the initial slopes of the fitted curves in Figs. 3 through 6 represent values of the product $(1 - B)K$. This quantity is shown as a function of particle size in Fig. 8 for all four hydrocarbons. A strong decrease with increasing average particle diameter is observed in each case.

Auger Analysis

As in previous work (*2, 3*), accumulation of carbonaceous decomposition products on the Pd crystallite surfaces was monitored using Auger electron spectroscopy. Due to the overlap of the 272-eV carbon peak with the 279-eV palladium peak, it was necessary to employ an indirect method of carbon detection; therefore, observations of the 330-eV/279-eV $dN(E)/dE$ Pd peak height ratio were recorded for increasing cumulative hydrocarbon exposure. Such results are illustrated in Fig. 9 for a sample treated with acetylene. The solid circles represent data points in a plot of the above peak ratio vs cumulative acetylene exposure for the particles. The downward sloping straight line is a linear least-squares fit to the data and is included to indicate the decreasing trend in the ratio as the cumulative acetylene exposure increases. This decreasing trend, which is due to the relative increase in the overlapping carbon signal, provides supporting evidence for the buildup of carbon-containing decomposition products.

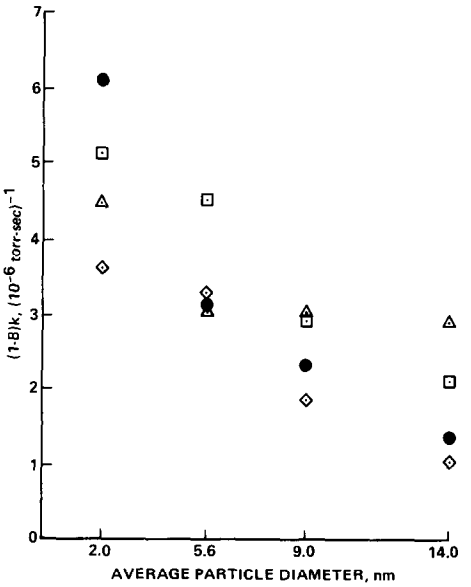

FIG. 8. Initial slope absolute values of solid curves in Figs. 3–6 for ethylene (squares), propylene (triangles), acetylene (diamonds), and methylacetylene (solid circles) vs average particle size. These slope values are equal to $(1 - B)k$ from the least-squares fits, with $B = 0$ for the alkynes. All decreases with increasing particle size shown here can be explained in terms of decreasing surface density of hydrocarbon decomposition sites with increasing particle size (see text).

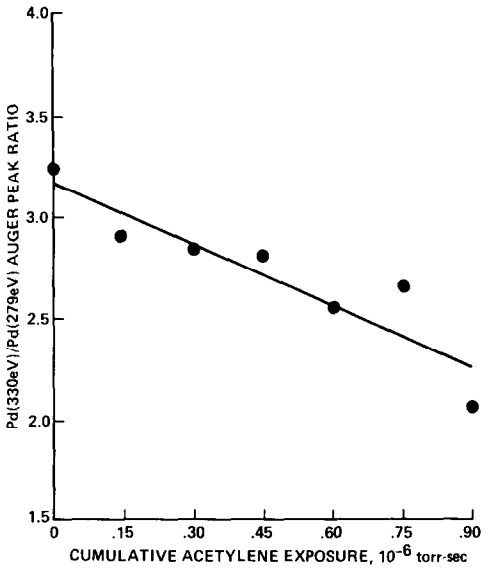

FIG. 9. Decrease in ratio of 330-eV $dN(E)/dE$ Pd Auger peak to 279-eV Pd peak (plus overlapping 272-eV carbon peak) with increasing cumulative acetylene exposure for 2.0-nm Pd particles illustrates AES observation of buildup of carbonaceous decomposition products.

DISCUSSION

The CO desorption peak area losses occurring in all series of hydrocarbon treatments establish that such treatments cause blocking of CO adsorption sites on the Pd particles. There is also considerable evidence in the literature that the hydrocarbon gases cause this blocking through decomposition rather than simple molecular adsorption. For example, recent EELS studies by Stuve *et al.* (*5*) revealed the formation of methylidyne groups (CH) when ethylene was annealed to 300 K after adsorption on Pd (100) at 80 K, and subsequent decomposition of the hydrocarbon to surface carbon upon heating to 500 K. Gentle and Muetterties (*6*) have recently described acetylene, ethylene, and benzene decomposition reactions occurring on the (111), (100), and (110) faces of Pd over a broad range of temperature by employing thermal desorption, Auger spectroscopy, and low-energy electron diffraction. Tysoe *et al.* have obtained evidence for the formation of a vinylidene species (with the C–C axis perpendicular to the surface) as acetylene adsorbs on Pd (111) at 300 K (*7*) and for ethylidyne as the room temperature phase produced by ethylene on Pd (111) (*8*). This last result supports findings previously reported by Kesmodel and Gates (*9*) in their high-resolution electron energy loss work, and by Lloyd and Netzer (*10*) using angle-resolved ultraviolet photoelectron spectroscopy which imply an adsorption/decomposition reaction.

Most significantly, Beebe and Yates (*11*) have directly observed CO adsorption site blocking by ethylidyne on Pd/Al_2O_3 systems using transmission infrared spectroscopy. It has been shown, furthermore, that ethylidyne formation also occurs at 300 K on Group VIII metals other than Pd (*12–16*).

Independently of the detailed mechanisms of the contaminating surface reactions or the temperature at which they occur, the above data imply certain conclusions concerning reaction site distributions and particle reactivity. The relatively successful fits of the CO adsorption area vs hydrocarbon exposure data (Figs. 3 through 6) suggested the following considerations. Let us consider three categories of surface sites on the Pd particles:

Type 1: Sites where hydrocarbon decomposition occurs. These may also adsorb CO molecules. We assume that after a hydrocarbon molecule decomposes at such a location, the site is deactivated with respect to both CO adsorption and further decomposition reaction.

Type 2: Neighboring CO adsorption sites which are associated closely enough with Type 1 sites that adsorption of CO is prevented at these nearby sites by the presence of hydrocarbon decomposition products from the Type 1 sites.

Type 3: CO adsorption sites at which CO adsorption is unhindered by hydrocarbon decomposition. They are presumably suffi-

ciently isolated (with respect to Type 1 sites above) to possess this property.

During a hydrocarbon dose at constant pressure, let M be the total number of uncontaminated Type 1 sites per unit area remaining on a sample at time t. The sample has at this time received a total hydrocarbon exposure $x = Pt$ Torr-sec at pressure P, where t is the accumulated dose time. The exponential loss of CO adsorbing area with exposure suggests an overall reaction that is first order in active site concentration, that is,

$$dM/dx = -kM, \tag{2}$$

which, when integrated, becomes

$$M(x) = M_0 \exp(-kx), \tag{3}$$

where M_0 is the initial number (at $t = 0$) of active Type 1 sites. Simply put, the active sites decay exponentially with exposure.

Let N_0 be the total number of CO adsorption sites per unit area on clean particle surfaces. Let q be the number of these sites blocked per decomposed hydrocarbon molecule. As a function of cumulative hydrocarbon exposure, x, the number, Y, of remaining CO sites per unit area will be

$$Y(x) = N_0 - [M_0 - M(x)]q. \tag{4}$$

Substituting Eq. (3) and rearranging give

$$Y(x) = qM_0 \exp(-kx) + N_0 - qM_0. \tag{5}$$

Normalizing this equation by dividing both sides by N_0,

$$y(x) = (qM_0/N_0) \exp(-kx) + (N_0 - qM_0)/N_0, \tag{6}$$

which is the same as Eq. (1) if we let $B = (N_0 - qM_0)/N_0$. Thus, within the interpretation of this model, calculations of the parameters k and B for a given sample correspond, respectively, to (a) the exponential decay constant of the Type 1 sites, and (b) the fraction of the initial total CO adsorption sites which are of Type 3. (As can be seen from Eq. (2), k is proportional to the probability that a hydrocarbon molecule will decompose as it impinges upon an active decomposition site.)

Clearly the different behavior exhibited by the alkynes ($B = 0$ and the stronger particle size dependence of k) when compared with the alkenes suggests that the decomposition sites for these gases may differ in an important way from those of ethylene and propylene.

For the two alkenes, a nonzero value of B implies that Type 1 sites and their associated Type 2 sites do not cover the entire surface of a particle. Some of the CO adsorbing area must be occupied by Type 3 sites. Such a situation is pictorially represented in Figs. 10a and 10b, where the dots represent Type 1 sites and the shaded areas around them represent their associated Type 2 sites. This set of figures has also been drawn to illustrate an explanation of the particle size dependence of the asymptotes (Figs. 3 and 4) and initial decays (Fig. 8) for propylene and ethylene. The closer packing of decomposition sites on the

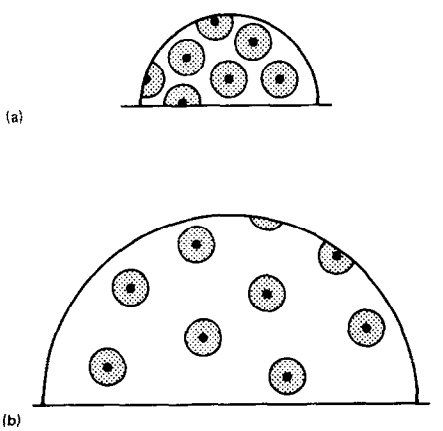

FIG. 10. Pictorial representation of surface site distribution on a small (a) and a large (b) Pd particle to be treated with ethylene or propylene. The relative isolation of hydrocarbon decomposition sites (dots) on both large and small particles is consistent with the particle size independence of the decay constant, k, for the alkenes in Fig. 7. On smaller particles, the greater proportion of Type 2 sites (shaded circles; see text) and lower proportion of Type 3 sites (unshaded area) account for the larger initial decay in CO adsorbing area due to olefin exposure (Fig. 8).

smaller particle (Fig. 10a) represents a greater surface density of such sites, leaving a smaller proportion of Type 3 sites (unshaded area), to give a smaller value of B. The combination of these conditions and the approximate particle size independence of the alkenes' k (as shown in Fig. 7) thus explains the ethylene and propylene data in Fig. 8. Smaller particles have more decomposition sites per unit area, and this accounts for their greater initial decays.

The fact that k is article size independent for ethylene and propylene supports the assumption that the Pd atom configurations comprising the sites are the same regardless of the particle on which they reside, and that the decomposition sites are isolated from each other to the extent illustrated in Figs. 10a and 10b. Since k is proportional to the probability that a hydrocarbon molecule will decompose at a Type 1 site, the exponential decays indicate that this probability is independent of decomposition product coverage.

The best-fit curves for the alkynes consistently indicate that $B = 0$. Therefore, the particles do not possess Type 3 sites with respect to these gases. Type 1 and Type 2 sites for acetylene and methylacetylene thus account for the entire initial CO adsorbing area, as depicted in Figs. 11a and 11b. Once again, the dots represent Type 1 sites and the shading Type 2 sites. For the sake of clarity, only a few of the Type 1 sites have their Type 2 domains (circles) drawn around them. Since each domain contains several neighboring Type 1 sites, each decomposing alkyne molecule contaminates several decomposition sites along with a number of Type 2 sites. In this situation, the decay constant, k, will increase in proportion to the average number of Type 1 sites per domain. (Assume here, too, that the physical nature of individual sites and domains is particle independent.) The vanishing of B and the particle size dependence of k for the alkynes in Fig. 7 can then be explained in terms of a greater surface concentration of decomposition sites

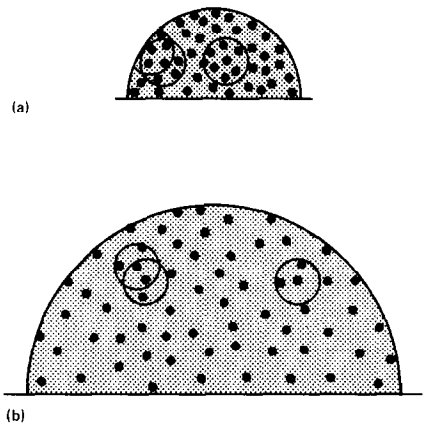

FIG. 11. Pictorial representation of surface site distribution on a small (a) and a large (b) Pd particle to be treated with acetylene or methylacetylene. The fact that all CO adsorbing sites can be contaminated, whether they are Type 1 (dots; see text) or Type 2 (shading), is implied by the zero asymptotes of the CO adsorption area decay for alkynes (Figs. 5 and 6). Contaminable regions (circles; only a few have been drawn for clarity) surrounding Type 1 sites contain more Type 1 sites on smaller particles. This is due to a greater surface density of Type 1 sites and accounts for the larger value of the CO adsorption area decay constant, k, for smaller particles treated with alkynes (Fig. 7).

on smaller particles as represented in Figs. 11a and 11b. All CO adsorption sites can be blocked by alkyne decomposition, and the higher concentration of decomposition sites on smaller particles is responsible for the greater decay constants of such crystallites.

It is also evident from Figs. 7 and 8 that the addition of a methyl group to either ethylene or acetylene does not significantly affect the decomposition behavior of either species. The important chemical difference between the gases studied appears to be that of the double vs triple carbon–carbon bond. The two different species must react with Type 1 sites bearing different relationships to their corresponding Type 2 sites, as discussed above. However, if site blocking were caused only by steric effects, it is unlikely that an extra methyl group would have a negligible influence. The data thus imply that, for Type 2 sites at least, the mechanism of deactivation is an electronic

effect which extends beyond the domain of simple physical blocking.

Finally, the decreases in initial active site concentrations implied in Fig. 8 can be compared to the statistics obtained from the geometrical models of Van Hardeveld and Hartog (*17*) for fcc crystallites. Considering the range of particle sizes studied, such a comparison implies that the decomposition sites for all hydrocarbons in these experiments are most probably edge sites.

CONCLUSION

The direct effects of metal–support interactions (for example, charge transfer which modifies electronic properties of particles, as opposed to the indirect effect of morphological change, affecting site distribution) introduce many physically complex questions and are not nearly as satisfactory when considered as alternative explanations of the above data. Several hydrocarbon reactions studied in the literature (*18*) suggest that such metal–support effects would cause a decrease in the activity of the smaller particles rather than the increase observed for alkynes. That direct metal–support effects could be so strongly operative for alkyne decomposition while absent in the cases of the alkenes is another unlikely property that stands as evidence against them.

The site-distribution model, however, provides a geometrical explanation for the behavior of the gases studied. It is attractive in that it invokes only a few simple and general assumptions about the nature of the gas–particle interaction. These assumptions are independent of the exact details of the reactions responsible for blocking surface sites. As can be seen, they account for the lower reactivity of larger particles in the decomposition of alkynes, and for the lower fractional loss of CO adsorption sites on larger particles due to the alkene decompositions, both in terms of decreasing active site concentration with increasing particle size.

REFERENCES

1. Doering, D. L., Dickinson, J. T., and Poppa, H., *J. Catal.* **73,** 91 (1982).
2. Durrer, W. G., Poppa, H., Dickinson, J. T., and Park, C., *J. Vac. Sci. Technol. A* **3**(3), 1545 (1985).
3. Doering, D. L., Poppa, H., and Dickinson, J. T., *J. Vac. Sci. Technol.* **17**(1), 198 (1980).
4. Durrer, W. G., Ph.D. thesis, University Microfilms International, 1987.
5. Stuve, E. M., Madix, R. J., and Brundle, C. R., *Surf. Sci.* **152/153,** 532 (1985).
6. Gentle, T. M., and Muetterties, E. L., *J. Phys. Chem.* **87,** 2469 (1983).
7. Tysoe, W. T., Nyberg, G. L., and Lambert, R. M., *Surf. Sci.* **135,** 128 (1983).
8. Tysoe, W. T., Nyberg, G. L., and Lambert, R. M., *J. Phys. Chem.* **88,** 1960 (1984).
9. Kesmodel, L. L., and Gates, J. A., *Surf. Sci.* **111,** L747 (1981).
10. Lloyd, D. R., and Netzer, F. P., *Surf. Sci.* **129,** L249 (1983).
11. Beebe, T. P., Jr., and Yates, J. T., Jr., *Surf. Sci.* **173,** L606 (1986).
12. Godbey, D., Zaera, F., Yeates, R., and Somorjai, G. A., *Surf. Sci.* **167,** 50 (1986).
13. Kesmodel, L., DuBois, L., and Somorjai, G. A., *J. Chem. Phys.* **70,** 2180 (1979).
14. Yu, R., and Gustafsson, T., *Surf. Sci.* **182,** L234 (1987).
15. Marinova, Ts. S., and Kostov, K. L., *Surf. Sci.* **181,** 573 (1987).
16. Greenlief, C. M., Radloff, P. L., Zhou, X.-L., and White, J. M., *Surf. Sci.* **191,** 93 (1987).
17. Van Hardeveld, R., and Hartog, F., *Surf. Sci.* **15,** 189 (1969).
18. Bond, G. C., *in* "Metal–Support and Metal–Additive Effects in Catalysis" (B. Imelik, *et al.*, Ed.), p. 1. Elsevier, Amsterdam, 1982.